Coventry
University

Coventry University Repository for the Virtual Environment (CURVE)

Available in the CURVE Research Collection: March 2012

Evaluation of SWIR–based methods for quantifying active volcano radiant emissions using NASA EOS–ASTER data

Authors:

MATTHEW BLACKETT †‡*
MARTIN J WOOSTER†

†Environmental Monitoring and Modelling Group, Department of Geography, King's College London, London, UK
‡Now: Environment, Hazards and Risk Applied Research Group, Department of Geography, Environment and Disaster Management, Coventry University, Coventry, UK

*Corresponding author. Email address: matthew.blackett@coventry.ac.uk

ABSTRACT

Analysis of thermally emissive volcanic features using satellite infrared remote sensing has been conducted over recent decades, primarily using shortwave and thermal infrared (SWIR; TIR) radiance data. The Advanced Spaceborne Thermal Emission and Reflection Radiometer (ASTER), mounted on the Earth Observation System (EOS) Terra satellite, offers an advance on earlier instruments, having more bands covering the SWIR atmospheric window and offering a wider dynamic range. This paper compares methods used to analyse ASTER SWIR imagery of active volcanoes, using both simulated cases and actual ASTER imagery of Lascar Volcano, and focusing on radiative power estimates. Those based on the Oppenheimer (1993) approach are found to be most reliable for simulated surfaces, with the Lombardo and Buongiorno (2006) and Dozier (1981) retrievals having larger uncertainties in most cases. However, the Dozier Method results in the highest proportion of successful retrievals, the reliability of which is influenced by factors including band combination, gain setting and saturation. The radiative power metric is shown as a more reliable measure than sub–pixel characterisations of hotspot temperature and area, as retrieved by these methods. We conclude with an assessment of ASTER in terms of its utility for providing quantitative observations of active volcanic surfaces.

1. Introduction

The infrared remote sensing of volcanic phenomena has been undertaken for a number of decades. Fisher *et al.* (1964) was amongst the first to describe early aerial infrared surveys of Hawaiian volcanoes. During the 1980s, the satellite remote sensing of volcanic thermal anomalies became the focus of more detailed studies (e.g. Francis and McAllister [1986]; Rothery *et al.* [1988]), while Glaze *et al.* (1989) showed that variations in such signals are of use in comparing activity between volcanoes. The field increasingly became a sub–discipline in its own right, with numerous studies harnessing its utility in, for example, examining fumarolic activity (Flynn *et al.* 1994; Wooster *et al.* 2000) and lava–dome behaviour (Oppenheimer *et al.* 1993; Carter *et al.* 2007), quantifying magma fluxes at lava–lakes (Harris *et al.* 1997), determining lava flow effusion rates (Harris *et al.* 1998; Lombardo *et al.* 2004) and mapping active volcanic craters (Blackett 2007). Chronologies of volcanic behaviour (Wright *et al.* 2005; Van Manen and Dehn 2009), attempts at observation automation (Davies *et al.* 2006) and hyperspectral investigations of lava flows (Lombardo *et al.* 2006; 2009) have also been conducted. However, despite these advances, Flynn (1996) highlighted that no operating satellite provides the required frequency of coverage, spectral resolution and dynamic range optimal for volcanic monitoring; this remains true today.

The Advanced Spaceborne Thermal Emission and Reflection Radiometer (ASTER), present on the Earth Observation System (EOS) Terra satellite, is one satellite remote sensing instrument for which the observation of active volcanoes was considered in its design (Yamaguchi *et al.* 1998; Pieri and Abrams 2004). This paper examines the methods available for quantifying volcanic activity using shortwave infrared (SWIR) radiance data from ASTER. The sensor, and the fundamentals of infrared remote sensing of thermally anomalous surfaces, are first introduced. This is followed by a discussion of the various methods commonly applied to analyse such data and which envisage the surface as displaying a multi–thermal component structure. These methods are applied to both simulated volcanic surfaces and to a six–year time series of imagery of Lascar volcano, Chile, enabling their assessment and intercomparison. Results from the optimum methods allow the more recent, and largely unreported, infrared emission variations at Lascar to be documented.

1.1 Infrared Remote Sensing

All objects above absolute zero (0 K) emit electromagnetic radiation, the wavelength and quantity of which are a function of the characteristics of the surface in terms of its temperature and radiating efficiency (emissivity). As the temperature of a surface increases, so too does the total radiated energy flux; this is according to the Stefan–Boltzmann Law (Stefan 1879; Boltzmann 1884):

$$E = \sigma T^4 \tag{1}$$

Where: E = total radiated energy flux (W m^{-2}), T = temperature of blackbody (K) and σ = Stefan–Boltzmann Constant (5.6697 x 10^{-8} W m^{-2} K^{-4}).

Trends of increasing spectral radiance with temperature are true for all wavelengths but, according to Wien's Displacement Law (Wien 1896), the peak wavelength of emission shifts to shorter wavelengths with increasing temperature (Rothery 1988), following:

$$\lambda_{max} = \frac{b}{T} \tag{2}$$

Where: λ_{max} = peak wavelength (m), T = temperature of a blackbody (K) and b = Wien's displacement constant (2.8978 x 10^{-3} m K).

In terms of spectral radiance therefore, the emissions from ambient to hot surfaces are greatest in the infrared, with those of very hot surfaces being enhanced in the SWIR and mid–

infrared (MIR) (1.6–3.0 µm and 3.0–8.0 µm, respectively) compared with those in the thermal–infrared (TIR) (8.0–15.0 µm) region. The overall spectral radiance, $L_\lambda(T)$, (in units of $W\,m^{-2}\,sr^{-1}\,m^{-1}$) of a blackbody at a particular temperature (T) and wavelength (λ), is given by the Planck Function (Planck 1901), which effectively summarises that the spectral radiance emitted from a surface will increase with its temperature, while the chief emissions will become of shorter wavelength (Donnegan and Flynn 2004):

$$L_\lambda(T) = \frac{C_1}{\lambda^5 \left(exp\left(\dfrac{C_2}{\lambda T} \right) - 1 \right)} \qquad (3)$$

Where: C_1 and C_2 = constants of 1.19 x 10^{-16} $W\,m^{-2}\,sr^{-1}$ and 1.44 x 10^{-2} m K, respectively (Wooster 2002).

The significance of these characteristics is two–fold. Firstly, a hot surface (at magmatic temperature, for example) will emit significant quantities of infrared energy compared to a cooler surface (particularly at shorter–wavelengths), even if it is relatively small or, indeed, sub–pixel in size. Secondly, when a surface of spatially varying temperature is imaged in the infrared, it will appear different depending on the wavelength used to image it. These characteristics have important implications for the infrared remote sensing of active volcanic surfaces. For example, since TIR bands are less sensitive to the hottest thermally anomalous surfaces, two TIR pixels may appear identical while actually viewing surfaces displaying different sub–pixel thermal components (Vaughan *et al.* 2010). This highlights the importance of using SWIR data for the highest accuracy when analysing active volcanic surfaces.

1.2 ASTER

Early hopes when ASTER was launched onboard the NASA Terra satellite in 1999 were that it would provide unprecedented volcanological observations (Pieri and Abrams 2004). It was the only instrument that would routinely acquire high–spatial resolution, night–time imagery of volcanic targets in both SWIR and TIR bands (Wessels *et al.* 2004). In this unique 'volcano mode' (Yamaguchi *et al.* 1998, p.1069), SWIR observations would be of particular utility due to the absence of sun–light contamination thereby aiding accurate quantitative analyses (Wooster and Kaneko 2001; Wright and Flynn 2004; Davies *et al.* 2006). Additionally, using night–time SWIR imagery would enhance the contrast between hot and ambient surfaces, thereby facilitating the isolation of even the smallest, but hottest, thermally anomalous surfaces (Harris *et al.* 1997). Other features of ASTER greeted optimistically by the volcanological community were, in large part, also associated with its SWIR observing capabilities, including:

- **Six–SWIR bands**, compared with just two on ASTER's predecessors (the Landsat Thematic Mapper [TM] and Enhanced Thematic Mapper [ETM+]). This provided for the observation of volcanic surfaces over a range of extreme temperatures.

- **A narrow SWIR spectral range**, compared with that of its predecessors. This theoretically enhanced the reliability of its temperature determinations due to the smaller flux uncertainties within given bandwidths (Hirn *et al.* 2005).

- **30 m spatial resolution**, making the sensor superior to many other polar orbiting sensors (and to all geostationary sensors) previously used in hotspot remote sensing (although the same as for Landsat ETM+). The chief advantage of this is the reduction in the inclusion of radiative contributions from surfaces of widely differing temperature (Pieri *et al.* 1995). It is also advantageous for hot–surface detection since, despite lacking the

'hotspot–optimised' spectral bands of MODIS (i.e. the thermally sensitive MIR bands), any hot–surface will likely cover a significant proportion of an ASTER SWIR pixel, resulting in substantial signals being detected for even the smallest hotspots (Morisette *et al.* 2005).

- **Normal–, high–, or two low–gain settings**, functioning by altering the range and amplification of the detected signals (Pieri and Abrams 2004). Low–gain settings reduce the occurrence of saturation by increasing the dynamic range (figure 1) and therefore, maximum radiance that can be detected (figure 2). This increases the possibility of obtaining quantitative volcanic observations at much higher pixel–integrated brightness temperatures (Donnegan and Flynn 2004). Low–gain bands however, are less sensitive to subtly radiant surfaces. It is unfortunate that despite their availability, low–gain settings appear not to have been widely used to observe thermally anomalous surfaces. Giglio *et al.* (2008) for example, note that only a small proportion of the ASTER SWIR imagery of fires that they studied had utilised the low–gain setting. The effect of this was that saturation was found to be common, and this also remains the case for volcanic observations.

FIGURE 1 HERE
FIGURE 2 HERE

Prior to its launch, and in an attempt to evaluate the much publicised potential of ASTER in observing volcanic phenomena, Wright *et al.* (1999) set out to simulate the sensor's SWIR response to volcanic targets. With its advantages over Landsat TM and ETM+, it was envisaged that ASTER would provide, simultaneously for almost the first time, up to six unsaturated bands of SWIR radiance measurements of thermally anomalous volcanic surfaces. The study determined, however, that saturation would still in fact be common, even when operating in low gain mode. The chief reason for this is that at the 30 m pixel size, even a relatively small scale anomaly would contribute disproportionately to the overall detected signal, e.g. saturation would be experienced when an area of freshly exposed lava approached just 1% pixel areal coverage (i.e. $9\,m^2$ of the $900\,m^2$ SWIR pixel). Consequently, Wright *et al.* (1999) suggested that unsaturated observations of features such as lava–lakes and open channel lava–flows would often be impossible. Based on this, they argued that sensors with a coarser spatial resolution (e.g. ATSR and MODIS), would remain useful due to their reduced tendency to saturate.

Despite ASTER having been in orbit for over ten years, few published studies have utilised its SWIR data for making volcanic infrared emission observations, and none have verified the suggestions by Wright *et al.* (1999). In a special issue of *Remote Sensing of Environment*, which focused purely on the scientific results of ASTER, of the fifteen papers, only one (Pieri and Abrams 2005) was concerned with volcanic observations and even this made no use of ASTER's SWIR observational capabilities. Pieri and Abrams (2004) introduce a number of possible volcanic applications and present examples of ASTER SWIR imagery, while Lombardo and Buongiorno (2006) and Davies *et al.* (2008) make comparisons between quantitative observations from the ASTER SWIR bands and, respectively, those from comparable bands of the Multispectral Infrared and Visible Imaging Spectrometer (MIVIS) airborne instrument and the EOS Hyperion sensor. Some studies have also attempted to retrieve volcanic surface temperatures using ASTER SWIR data (e.g. Carter et al. 2008) and to integrate SWIR observations of volcanic eruptions with both field, and other satellite sensor, observations (e.g. Carter et al. 2008; Rose and Ramsey 2009). This arguably limited range of studies suggests that a thorough investigation of the volcanological utility of ASTER's SWIR bands is outstanding. Such an investigation is made all the more relevant as the Terra satellite has now exceeded its design lifespan and its SWIR bands no longer function (Wooster 2007; Vaughan *et al.* 2010).

1.3   Satellite Observations of Volcanic Surfaces

In terms of viewing Earth's surface, the finest detail which satellite sensors can resolve depends on the spatial resolution (i.e. pixel size) of the sensor. The radiance measured within a pixel is that *averaged* over its whole area, so signals from sub–pixel thermal components are combined into a single 'pixel–integrated' value (Francis and Rothery 2000). When imaging an active lava–flow for example, one pixel may include radiance from numerous different surface components, including both incandescent and cooler lava–flows, and surfaces unaffected by volcanic heating. Being of differing temperature, each of these components will emit different amounts of electromagnetic radiation at a particular wavelength, with the resulting signal combined to provide a 'pixel integrated' signal.

Given multispectral data, each waveband of which will be most sensitive to the radiant emissions from surfaces at a particular temperature, it is possible to make assumptions about a surface being viewed in terms of its constituent thermal components. This was first recognised in Dozier (1981) and Matson and Dozier (1981), which showed that, for observations of sub–pixel hotspots, if the spectral radiant emissions of a pixel are known in two suitably separated, thermally sensitive wavebands, then its two–component sub–pixel thermal structure (e.g. figure 3) can be estimated. This is calculated via use of two non–linear, simultaneous equations that quantify the radiant energy emissions from each component:

$$R_x = P_h \, L_x(T_h \,) + [(1 - P_h \,) \, L_x(T_c \,)] \tag{4}$$

$$R_y = P_h \, L_y(T_h \,) + [(1 - P_h \,) \, L_y(T_c \,)] \tag{5}$$

Where: R_x and R_y = spectral radiance detected by a remote sensor in bands x and y ($W\,m^{-2}\,sr^{-1}\,\mu m^{-1}$), adjusted for atmospheric transmissivity and surface emissivity; P_h = the proportion of the pixel occupied by the hotspot; $L_x(T_h)$ and $L_y(T_c)$ = the spectral radiance (L, $W\,m^{-2}\,sr^{-1}\,\mu m^{-1}$) emitted in a particular band (x or y) by a surface at temperature T_h (the hot component) or T_c (the cooler component), as determined by the Planck Function (equation [3]).

FIGURE 3 HERE

Since this method uses two equations and there are three unknowns (T_h, T_c and P_h), its application requires one more piece of information, and either T_h or T_c are usually assumed. In assuming only two thermal components, the Dozier Method (often termed dual–band method) will only ever *approximate* reality, although such assumptions will, of course, be more realistic than the assumption of a single, uniform, pixel–wide temperature structure as envisaged in earlier studies, e.g. Shaw and Swanson (1970), Danes (1972) and Dragoni *et al.* (1986).

Amongst the first terrestrial volcanological applications of the dual–band method was Rothery *et al.* (1988) which examined satellite imagery of various volcanic phenomena. This work followed Dozier (1981) in assuming the cooler component temperature (T_c), based on the assumption that its contribution to the overall pixel radiance would be small as a result of Planck's Law (equation [3]) (Donnegan and Flynn 2004). However, Oppenheimer (1991) determined that the emissions from the cooler component were more significant than had been previously suggested, reasoning that although radiant energy emissions are locally high from regions of exposed hot core, they are typically small when compared with those from the often much larger surrounding 'cooler crust' region. In the absence of other information, evidence therefore suggested it is more justifiable to *assume* T_h (as something close to the magmatic temperature) in dual–band calculations and, in turn, to *calculate* T_c.

Based on field spectro–radiometer studies at Pu'u O'o, Hawaii, Flynn (1992) recognised that volcanic surface models assuming three–thermal components actually provided a significantly more accurate surface characterisation than two component models. This third component was assumed to have a temperature between T_h and T_c (Flynn and

Mouginis–Mark 1992). Building on the dual–band approach, and harnessing Thematic Mapper Simulator (TMS) imagery of Mount Etna, Oppenheimer (1993) presented a procedure utilising *three*–infrared bands to derive three–component pixel models (figure 4). For the application of this method, where all three bands are located in the SWIR spectral region, and where the ambient background temperature (T_b) is too cool for significant SWIR emittance (i.e. < 100 °C), the following equation set is given:

$$P_h = \frac{R_x L_1(T_c) - R_1 L_x(T_c)}{L_x(T_h)L_1(T_c) - L_x(T_c)L_1(T_h)} \tag{6}$$

$$P_c = \frac{R_1 - p_h L_1(T_h)}{L_1(T_c)} \tag{7}$$

Where: R_x = spectral radiance in band x ($W\,m^{-2}\,sr^{-1}\,\mu m^{-1}$), band x = band 2 and/or band 3 of the 3 bands being used and R_1 = spectral radiance in the first band of the three being used ($W\,m^{-2}\,sr^{-1}\,\mu m^{-1}$).

FIGURE 4 HERE

Lombardo and Buongiorno (2006) re–examined and updated the dual–band method, presenting a new procedure which can retrieve a *two*–component solution via three equations using *three*–SWIR bands. The rationale for this was that, in contrast to both the aforementioned Dozier and Oppenheimer Methods, it removes the requirement for an assumed temperature since there are three–equations and three–unknowns:

$$R_x = P_h (L_x, T_h) + [(1 - P_h)(L_x, T_c)] \tag{8}$$

$$R_y = P_h (L_y, T_h) + [(1 - P_h)(L_y, T_c)] \tag{9}$$

$$R_z = P_h (L_z, T_h) + [(1 - P_h)(L_z, T_c)] \tag{10}$$

Where: $R_{x,y,z}$ = spectral radiance detected by a remote sensor in bands x, y or z ($W\,m^{-2}\,sr^{-1}\,\mu m^{-1}$).

Lombardo and Buongiorno (2006) demonstrate, by applying this equation–set to MIVIS imagery of an Etnean lava–flow and allowing T_h to vary unconstrained until a solution is reached, that T_h varies across a volcanic surface. This, they argue, confirms that the dual–band technique, utilising a single T_h value, might not always provide reliable results.

These methods provide a *characterisation* of the surface being viewed (in terms of effective hotspot area and temperature) but by themselves provide no indication of the radiative power emission. In contrast, total radiative power (integrated over all wavelengths) is, perhaps, more useful for characterising volcanic activity and for facilitating effective volcano inter–comparisons; it was also found by Wright and Flynn (2003) to be a more accurate and consistent measure. The reason for this enhanced accuracy is that, in general, errors in hotspot temperature act in a different direction to those in hotspot area (i.e. when one is overestimated the other is usually underestimated). Therefore, to some extent, these errors cancel each other out when used to derive the total radiative power output. This value can be calculated via the Stefan–Boltzmann Law (equation [1]), using the following equations applied to either a two– or three–thermal component pixel:

$$Q = \sigma \varepsilon A [P_h T_h^{\,4} + (1 - P_h)T_c^{\,4}] \tag{11}$$

$$Q = \sigma \varepsilon S [P_h T_h^{\,4} + P_c T_c^{\,4} + (1 - P_h - P_c)T_b^{\,4}] \tag{12}$$

Where: Q = emitted radiant power (W), σ = Stefan–Boltzmann Constant (5.67 x10^{-8} W m^{-2} K^{-4}), ε = surface emissivity (unit–less) and A = pixel surface area (m^2).

This review has highlighted the potential advantages and disadvantages in the ASTER SWIR observation of thermally active volcanoes, and has presented the different approaches available to analyse these signals. A set of previously unanalysed ASTER night–time observations of Lascar Volcano (Chile), made over a six–year period (2000–2005), will now be used to assess the actual capability of these approaches when applied to real ASTER imagery of an already well–studied active volcanic target that has been analysed with data from TM, ETM+, ATSR and other infrared–capable sensors (e.g. Francis and Rothery 1987; Oppenheimer *et al*. 1993; Wooster and Rothery 1997; Wooster 2001).

2.   Methods

2.1   Study area and data acquisition

Lascar volcano is located in the northern Chilean Andes and is the most active volcano in the region (Oppenheimer *et al*. 1993). The summit at 5592 m consists of five overlapping craters, only one of which remains active (Tassi *et al.* 2009). Lascar's largest recorded eruption was in 1993 which resulted in localised pyroclastic flows and ash fallout over Buenos Aires, some 1500 km downwind (Wooster and Rothery 1997). More recently, the volcano erupted in 2006 and 2007 (BGVN 2006; 2007). A SWIR image of Lascar from 2003, obtained in daylight for greater detail, is displayed in figure 5.

FIGURE 5 HERE

ASTER data were acquired in two formats for use in this work: Level–1A (L1A) and Level–1B (L1B). L1A products are essentially unprocessed, while the L1B products are supplied calibrated and with all bands geometrically co–registered (Hellman and Ramsey 2004; Kato *et al.* 2001). Both product formats include data from ASTER's three telescopes (VIS/SWIR/TIR) and cover a ground area of 60 km x 60 km. In this work, L1A scenes were calibrated and geo–corrected to the equivalent of L1B and, following the removal of scenes for which no bands were set to low–gain, and/or which displayed extensive cloud cover at the active volcanic summit, a usable dataset of 32 images (from an original 91), with an average frequency of 8 images yr^{-1}, was generated (table 1).

TABLE 1 HERE

2.2   Data Pre–processing

The effects of both surface emissivity and the atmosphere on infrared observations must be accounted for to obtain an accurate estimation of surface emissions. In terms of emissivity, measured values often vary significantly for the same surface and over the area of one pixel. Added complications include the fact that emissivity varies with wavelength (Salisbury *et al.* 1988), rock age and (it is assumed) temperature (Flynn *et al.* 2001). With regard to Lascar, a surface emissivity of 0.91 was used in this work, agreeing with that published in Salisbury and D'Aria (1992) of 0.90–0.91 for andesite and rhyolite, and comparable to values used in other work (e.g. 0.92 in Wooster and Rothery 1997).

The most practical way to determine atmospheric transmissivity is to simulate local atmospheric conditions (Qin *et al.* 2002), and here this was conducted using seasonal radiosonde data taken from Antofagasta, Chile (273 km west of Lascar) and the MODTRAN radiative transfer code. The resulting atmospheric transmissivities for the ASTER SWIR bands are summarised in table 2.

TABLE 2 HERE

Additional pre–processing steps were also required because, in many cases, the apparently thermally anomalous region identified extended over a significantly larger area than the emitting lava dome itself (which is 150–400 m in diameter [Wooster *et al.* 1998]). This was particularly the case in ASTER SWIR bands set to high gain mode, in which it extended over 600 m from the radiant lava dome in all directions (and hence outside of the active crater) (figure 6). This spread signal was small in value (often little more than background noise) and this, coupled with its spread away from the lava dome feature, suggests it is most likely the result of signal bleeding into adjacent pixels, and not of true activity at the surface and indeed, even if it were, due to its small magnitude, it omission would not have significantly affected the resulting retrievals. As such, a thresholding approach was applied to extract the pixel signals directly attributable to the lava dome itself (here, these pixels are termed a cluster), and to exclude the elements of spread signal. The extracted volcanic surface emissions were then quantified by applying the equation below to the data associated with each pixel of the cluster; the mean $L_\lambda(T)$, averaged over all volcanic pixels, then acted as a single measure of the volcanic surface signal:

$$L_\lambda(T) = \frac{R_\lambda}{(\varepsilon_\lambda \tau_\lambda)} \qquad (13)$$

Where: R_λ = spectral radiance detected by a sensor ($\mathrm{W\,m^{-2}\,sr^{-1}\,\mu m^{-1}}$), τ_λ = atmospheric transmittance (unit–less); ε_λ = spectral emissivity of the radiating surface at wavelength λ (unit–less) and $L_\lambda(T)$ = actual spectral radiance emitted from the surface at temperature T ($\mathrm{W\,m^{-2}\,sr^{-1}\,\mu m^{-1}}$).

An additional complication found in relation to night–time SWIR ASTER imagery of volcanoes is that the gain setting of all bands was commonly not identical within the same scene. Bands 4, 6 and 8 were often set to the second low gain setting while bands 5, 7 and 9 were set to high gain. This is the standard volcano observation mode, set to ensure that unsaturated data are available in some bands when viewing an active volcano, while also ensuring that useful data remain available if viewing a volcano (and its surroundings) in a dormant state (Pieri 2005, pers. comm.). Due to the enhanced sensitivity of the high–gain bands, the 'thermally anomalous' region was disproportionately large in these bands (figure 6), and pixel saturation was more common (figure 7). Saturation effectively places a ceiling on the radiance that individual pixels can record, resulting in radiance underestimations. In fact, when radiative power retrievals for corresponding saturated and unsaturated imagery are compared for the Lascar time series examined here, where both sets of solutions are available (n=10), saturation resulted in an average underestimation of 36%, with a maximum underestimation of 71% in relation to scene number 8. Due to these effects, data obtained in high–gain were not utilised in this analysis.

FIGURE 6 HERE
FIGURE 7 HERE

2.3   *Radiant Emission Quantification*

The Dozier method was applied to the mean pixel radiance value of each cluster and for all combinations of SWIR low–gain bands (4–6, 4–8 and 6–8), with the radiative power emission subsequently calculated using equation (11). Similarly, the Oppenheimer and Lombardo and Buongiorno methods were applied, but with only three reliable bands of data, only one band combination was possible (4–6–8). With regard to the Oppenheimer method, retrievals both including and omitting signals from the background area were calculated. The radiative power retrievals were then multiplied by the number of pixels within each delimited cluster, thereby retrieving a value representing the entire anomalous surface. Where necessary, the

temperature of the hot component was assumed to be 1073 K, a temperature lower than the hottest lava temperatures (~ 1400 K [Lombardo and Buongiorno 2006]) in order to represent the dacitic composition of the dome, and higher than that of the cracks in the cooled carapace of lava domes (which may be from ambient to ~ 675 K [Fink 1990, in Wooster and Rothery 1999]). The implications of temperature uncertainties are investigated later. It should be noted that for some imaged scenarios, neither Dozier, Oppenheimer nor Lombardo and Buongiorno methods were successful in retrieving details about the surface being viewed. In these cases, no solutions were possible.

## 3.	Results

Results for both surface characterisation and radiative power values are presented here. Past work (e.g. Wright and Flynn 2003) has suggested that radiative power is the most reliable metric, a fact tested here by examining retrieval sensitivities to assumed T_h values, for three ASTER scenes and based on use of the dual–band combination of ASTER SWIR bands 4 and 6. It was found that by varying T_h between 875 and 1275 K resulted in P_h variations of over 600% (with corresponding T_c variations of little more than ±10%). However, as retrievals of P_h and T_c are inversely related, these sensitivities counteract one another and, in this case therefore, provided radiative power values varying within a maximum ±40% limit over the same T_h range. Consequently, the assumption that the radiative power metric is less sensitive to uncertainties in T_h appears correct, confirming it as a more reliable metric.

With regard to the Dozier method sensitivity to wavebands used, we found radiative power retrievals to vary by between 2 and 120% (mean of 34%), depending on the band combination (figure 8). This confirms the suggestion of Giglio and Justice (2003) in relation to fires, that the Dozier method retrievals are strongly dependent on observation wavelength. To determine one retrieval value for a particular scene against which radiative retrievals of this method could be compared with those of other methods for the same scene, the mean of all successful retrievals, irrespective of band combination, was calculated. This follows the method of Vaughan et al. (2010) which was applied in relation to surface characterisation values. These values are compared with those following the application of the Oppenheimer and Lombardo and Buongiorno methods in figure 9. It will be evident that retrievals of the two component methods agree well, while those of the Oppenheimer Method diverge significantly, with retrievals less common and, on average, 2.7 times larger. This corroborates the assertion of Oppenheimer (1993) of dual–band method overestimations on the order of 3–4 times.

FIGURE 8 HERE
FIGURE 9 HERE

To investigate these discrepancies, pixels imaging eight modelled volcanic surfaces were simulated with varying numbers of thermal components (4–7) at differing temperatures (300–1073 K) and with differing proportional areas (0.00001–0.75) (see table 3) (assuming an emissivity of 1.0). The true spectral radiance that such surfaces would emit was determined using Planck's Law (see equation [3]) and input into applications of the Dozier (using equations [4] and [5]), Oppenheimer (using equations [6] and [7]) and Lombardo and Buongiorno (using equations [8], [9] and [10]) Methods (in the case of the Oppenheimer Method, emissions from the background surface were also considered). The resulting retrievals are compared with values of the 'true' radiative power that such surfaces would produce in figure 10. In all cases, the retrievals encouragingly followed the same trends, although the Oppenheimer Method retained the most accurate retrievals, differing by a maximum of 21% from the "truth"; this was followed by the Lombardo and Buongiorno Method which delivered power overestimations of 11.4–70.6%. The Dozier Method was found to be the least reliable, overestimating by 44.4–107.8%. This appears to confirm the findings of Wright and Flynn (2003) that modelling a greater number of thermal components will better characterise the emissions from a volcanic surface. Surprisingly however, this

appears not always to be the case with radiative power being more accurately retrieved with the use of the two–component Lombardo and Buongiorno Method in relation to the six–component Model 6 scenario. Figure 10 also plots the radiative power values that would be calculated were the pixel–integrated values from ASTER's SWIR band 9 used (i.e. a value averaged for the whole pixel area based on ASTER band 9 emissions). The much greater deviation of these latter retrievals from the 'true' confirms the additional utility of these multi–band techniques in the quantitative analysis of active volcanic surfaces.

FIGURE 10 HERE
TABLE 3 HERE

Although seemingly producing the most reliable results, the chief disadvantage of the Oppenheimer Method (as with the Dozier Method) is its requirement for the assumption of T_h. The influence of varying T_h assumptions on retrievals of this method is presented in figure 11, for all Lascar time–series data (from table 1). After noting that retrievals are not always possible for all values of assumed T_h, a decline in radiative power retrieval with increasing T_h is apparent and is largely a result of the concurrent fall in retrieved P_c and rise in retrieved P_b. As P_c contributes significantly to the overall radiant power emission of such surfaces, and as P_b contributes only subtly, these relative changes reduce the total retrieval. Overall, where 700 K $< T_h <$ 1200 K was assumed, Oppenheimer Method retrievals were found for 25% of Lascar scenarios; this is in comparison to just 12.5% where T_h was fixed at 1073 K.

FIGURE 11 HERE

With Oppenheimer Method retrievals varying significantly with assumed T_h, perhaps the most justifiable way to present these is in terms of the range within which possible solutions lie following the assumption of a range of T_h values. Such results are displayed in table 4 for the ASTER Lascar time–series. Where the background signal is included, the average increase in radiative power retrieval following the assumption of a decreasing T_h of 1200–1000 K is 46%. Although the solutions vary more significantly than this for some dates, the acceptance of uncertainty by the depiction of a range of possible solutions is arguably more justifiable than prescribing a single value. Interestingly however, the mean of the retrieved power values in table 4 (where emissions from the background component are included), plotted against corresponding Dozier Method retrievals, shows a relatively strong relationship (figure 12). Retrievals of the Oppenheimer Method are however, on average, 47% smaller.

FIGURE 12 HERE
TABLE 4 HERE

The cause of the discrepancy between the Dozier and Oppenheimer Method retrievals is that methods utilising two bands of data attempt to quantify emissions from an entire surface (assuming it all to be thermally anomalous to a greater or lesser extent, i.e. figure 3) while those utilising three bands categorize a pixel as having three components, only two of which are significantly radiant in the SWIR (figure 4). The Dozier Method resulted in successful retrievals for 87.5% of Lascar scenarios examined, compared with just 25% for the Oppenheimer Method. Despite resulting in an increased retrieval rate, the apparent overestimation attributable to the Dozier Method limits its reliability. However, the strong relationship between its retrievals and those of the Oppenheimer Method (figure 12) provides the possibility that the more common Dozier Method retrievals could be corrected for their inherent overestimations.

In terms of a comparison between Lombardo and Buongiorno and Dozier Method radiative power retrievals, the relationship is relatively good, with figure 13 comparing the retrievals of both these methods for the Lascar time–series. One problem with the application of the Lombardo and Buongiorno method applied here, however, is that the authors suggest TIR data should be used to pin–point a more reliable solution. These data were not used in

this work due to the pixel size differential and misalignment between the ASTER SWIR and TIR telescopes (Yamaguchi *et al.* 2001; Iwasaki and Fujisada 2005). Consequently, the reliability of radiative power and surface characterisation retrievals from application of the method here may be, arguably, questionable.

FIGURE 13 HERE
3.1 The Lascar Time–series

Lascar has been intensively studied by satellite, including in the early Landsat TM studies of Francis and Rothery (1987) and Oppenheimer *et al.* (1993). Work has focused on this particular volcano for a number of reasons, including: its remote, desert location and high altitude (which make field studies difficult but often provide cloud–free views); its propensity to display hazardous Vulcanian to Plinian eruption styles (Matthews *et al.* 1997); its emission of significant quantities of heat from its lava dome (e.g. figure 5) and the cyclical behaviour in terms of emitted radiance, that it has been shown to display (Wooster and Rothery 1997; Matthews *et al.* 1997).

Based on the six–year ASTER SWIR imagery time–series, figure 14 depicts the corresponding Oppenheimer and Dozier Method radiative power retrievals attributed to Lascar. Despite its temporal inadequacy (due to ASTER's revisit frequency and, in the case of the Oppenheimer Method, its common failure to retrieve solutions), patterns are evident with both peaks and troughs and a general downward trend. It appears for example, that heightened signals were present at the start of the time–period which ended in a peak in June 2002; following this, there began a downward trend in emissions This figure also shows the main, albeit small, events occurring at the volcano over the time–period displayed. Point (a) corresponds with a number of small ash eruptions on 26 and 27 October, 2002 and point (b) with the emission of fine ash from fumaroles on 9 December, 2003 (BGVN 28:03 2003 and BGVN 29:01 2004 respectively). There appears to be no reflection of either of these events in the radiative power data, and this is likely to be the result of inexact image concurrency.

FIGURE 14 HERE

Evidently, despite the length of this time–series, its sparseness prevents conclusions from being drawn with regard to relationships between retrieved power, and specific volcanic events. This corroborates the findings of Vaughan and Hook (2006) who similarly found the temporal resolution of ASTER to be too low for the adequate monitoring of thermal changes at Mount St. Helens. The sparseness of observations at Lascar is, of course, also exacerbated by a scarcity of on–the–ground observations against which they might be compared. Significantly, this dataset provides little evidence for the cyclical behaviour that was postulated using pre–1993 data in both Wooster and Rothery (1997) and Matthews *et al.* (1997) and it therefore supports the suggestion of Aguilera (2005) that these cycles halted after the volcano's 1993 eruption. However, the decreasing trend in radiated energy over the period does corroborate the findings of Tassi et al. (2009) which suggest a decrease in fumarolic degassing between 2002 and 2006, which is attributed to decreasing inputs of magmatic fluids.

3.2 Assessment of ASTER

The ASTER instrument was planned to offer unprecedented volcanological observations (Pieri *et al.* 1995). Its arrival was greeted optimistically within the volcanological community due to its claimed utility in the "analysis of thermal properties of summit lakes, eruption plumes, and fumaroles, and investigation[s] of volcano lithology", (Mouginis–Mark *et al.* 1991, pg. 4). Indeed, the sensor's SWIR bands have been used in various enlightening volcanic studies (e.g. Pieri and Abrams 2004; Lombardo and Buongiorno, 2006; Carter et al. 2008; Davies et al. 2008; Rose and Ramsey 2009) and it is unfortunate for the field of volcanological remote sensing that they no longer function. However, despite these

unprecedented advantages, in relation to ASTER's SWIR bands some weaknesses for certain applications (as determined from the findings presented here) include: 1) its temporal resolution, which reduces its utility both in the long term monitoring of, and in the immediate response to, volcanic phenomena, and 2) the pattern of its gain settings, in terms of their alternating regime and their incapability to always provide unsaturated data.

Based on pre–launch simulations, Wright *et al*. (1999) predicted that saturation would occur in ASTER SWIR imagery of active lava–lakes and lava–flows. This has been confirmed here, even finding saturation occurring in low–gain imagery of less widespread and radiant volcanic features (i.e. the Lascar lava–dome). Despite this however, ASTER's low–gain SWIR bands did function to reduce the occurrence of saturation in many cases. For example, in relation to the ASTER Lascar time–series, the mean proportion of saturated pixels in low–gain imagery was 1.0% compared with 49.0% in corresponding high–gain imagery (figure 7). Where saturation could not be prevented, its effect (and that of the corresponding recovering pixels) on radiative power retrievals has been particularly highlighted, being shown to result in significant radiative power underestimations (by up to 36%).

In the majority of the ASTER SWIR night–time imagery examined, the band gain–settings alternated between low– and high–gain in neighbouring spectral channels. This regime has undoubtedly paved the way for the acquisition of volcanic imagery for a wider range of surfaces than would otherwise have been available. For the visualisation of volcanoes in an active state however, such a regime reduces the quantity of data available for analysis by increasing the occurrence of saturation and rendering data from bands of differing gain setting as incomparable; in such cases, the use of consistent (and low) gain–settings would have arguably been more useful. Mis–alignment between the SWIR and TIR telescopes, and the associated differences in pixel size, also prevented the quantitative use of imagery simultaneously acquired using these different parts of the spectrum.

The ASTER SWIR platform is capable of being pointed off nadir (for example, to view active volcanoes), resulting in a latitude-dependent revisit frequency of five–days or better (Pieri and Abrams, 2004). Under normal circumstances however, the platform's nominal revisit frequency is 16 days (Ramsey and Dehn 2004). This is adequate for many volcanic observations however, for monitoring dynamic volcanic processes, Wright *et al*. (2004) and Ramsey and Dehn (2004) show such a temporal resolution to be inadequate. This has been confirmed here with an attempt at analysing the long–term behaviour of Lascar Volcano using a six–year time–series of ASTER data. In relation to this time–series, the temporal inadequacy was compounded by the fact that not all of the imagery acquired was of usable quality (e.g. due to saturation or cloud–cover). This time–series arguably displayed an adequate temporal resolution for the determination of some trends, but was inadequate for deriving direct relationships with specific, on–the–ground events.

4.   Discussion

The utility of the Dozier (1981), Oppenheimer (1993) and Lombardo and Buongiorno (2006) Methods in terms of providing a quantification of volcanic activity based on ASTER imagery, is confirmed. Oppenheimer Method retrievals are found to produce the most reliable estimations of radiative power emission, with those of the Lombardo and Buongiorno and Dozier Methods overestimating it by up to 71% and 108%, respectively. However, the Dozier Method results in the highest proportion of successful retrievals i.e. the greatest number of scenarios for which a solution could be derived. The reliability of all solutions is shown to be strongly influenced by factors including: band combination (causing Dozier Method retrievals to differ by up to an average of 34%), gain setting (reducing numbers of reliable retrievals) and saturation (resulting in average Dozier Method retrieval underestimations of 36%). Despite these influences on radiative power retrievals, this metric itself is found to be a more reliable and stable measure than volcanic sub–pixel characterisations of hotspot temperature and area. The assumed hot–component temperature is also shown to influence retrievals,

suggesting that radiative power retrievals should be given only with any corresponding assumed hot component temperature(s).

The ASTER sensor has many advantages over its predecessors in relation to volcanological remote sensing, including its number of SWIR bands and their potential to be set at low–gain, and its pointing capabilities. In this work however, ASTER's temporal resolution has been shown to be sub–optimal for routine volcanic observations, with the six–year time series of SWIR imagery of Lascar examined in this work being shown to be rather sparse. In relation to the monitoring of active volcanic surfaces, the common alternating band gain setting also reduced the utility of the sensor's otherwise useful SWIR bands. Hopefully, the next generation of multispectral instruments will be improved along these lines and will be able to provide high spatial and, higher temporal, resolution observations, with better alignment between telescopes and higher (and consistently set) limits of saturation.

The currently flying Hyperion imaging spectrometer and Advanced Land Imager (on–board NASA's EOS–1 satellite) have effectively replaced ASTER as a source of SWIR volcanic observations. Hyperion, for example, possesses 220 bands in the 0.4–2.5 μm (VNIR–SWIR) region, at the same spatial resolution as ASTER's SWIR observations, making it well suited for detecting the heat emissions from volcanic activity and for providing unsaturated observations of even the hottest/most radiant surfaces (Davies et al. 2006; Wright et al. 2010). The prospects for the future are largely focused on the NASA Hyperspectral Infrared Imager (HyspIRI) mission which is planned for launch between 2013–2016 and which has volcanoes and natural hazards as one of its three top–level science questions for research (JPL, 2010). Similarly to Hyperion, this sensor is planned to possess a VNIR–SWIR (0.5–2.4) hyperspectral instrument with 220 bands (although at a spatial resolution of 60 m); its chief advantages are its corresponding 60 m TIR scanner that would be completely aligned with the SWIR imager (providing for a much wider spectrum of comparable observations of the surface), its cross–track pointing capability (providing for a repeat coverage of up to 3 days) and potentially on–board processing (meaning only relevant SWIR imagery need be downloaded and via a direct–broadcast link) (JPL, 2010; Chien et al. 2010).

5.   Conclusion

The utility of ASTER's SWIR bands studying volcanic behaviour has been confirmed in this study in relation to a six–year timeseries of imagery of the Chilean volcano, Lascar. Three methods for quantifying such observations have been examined, having been applied to both the timeseries of Lascar data and to modelled volcanic surfaces. The usefulness of each method (Dozier 1981; Oppenheimer 1993; Lombardo and Buongiorno 2006) has been exemplified in relation to both modelled and true volcanic surfaces, with each providing more accurate radiative power retrievals than would be calculated using just one band of data, although for most modelled cases the Oppenheimer (1993) method appears most accurate. The often significant influence of band combination used in relation to the Dozier method , is also demonstrated. Where each of these methods are applied, their retrievals in terms of surface characteristics (proportions of the pixel at different temperature) are shown to be less reliable metrics than using these retrievals to calculate the corresponding radiative power emission via the Stefan Boltzmann Law. Analysis of these radiative power retrievals for the Lascar timeseries revealed a decreasing trend in radiated energy from 2001–2005, corroborating the findings of other studies. Some shortcomings of the ASTER SWIR dataset have been highlighted with regard to the observation of thermally anomalous surfaces, although it appears a number of these have been addressed in the design of later sensors or have informed the design of future planned sensors.

References

ABRAMS, M., HOOK, S. AND RAMACHADRAN, B., 2002, *ASTER User Handbook*, Version 1, Jet Propulsion Laboratory, Pasadena, CA.

AGUILERA, F.,2005, Contrasting styles of volcanic activity as observed by remote sensing: The cases of Lascar, Llaima and Villarica volcanoes, Chile. In *6th International Symposium on Andean Geodynamics,* 2005*,* Barcelona, Extended Abstracts, pp. 21–25.

BGVN, 2003, Global Volc. Network. Lascar. Smithsonian Institution *Bulletin of the Global Volcanism Network*, 28:03, 03/2003.

BGVN, 2004, Global Volc. Network. Lascar. Smithsonian Institution *Bulletin of the Global Volcanism Network*, 29:01, 01/2004.

BGVN, 2006, Global Volc. Network. Lascar. Smithsonian Institution *Bulletin of the Global Volcanism Network*, 31:04, 04/2006.

BGVN, 2007, Global Volc. Network. Lascar. Smithsonian Institution *Bulletin of the Global Volcanism Network*, 32:09, 09/2007.

BLACKETT, M., 2007, Infrared Radiance of Mount Etna, Sicily. *Journal of Map Student Edition*, **v2007**, pp. 23–31.

BOLTZMANN, L., 1884, Ableitung des Stefan'schen Gesetzes, betreffend die Abhängigkeit der Wärmestrahlung von der Temperatur aus der electromagnetischen Lichttheorie. *Annalen der Physik und Chemie*, **22**, pp. 291–294.

CARTER, A. J., RAMSEY, M. S. AND BELOUSOV, A. B., 2007, Detection of a new summit crater on Bezymianny Volcano lava dome: satellite and field based thermal data. *Bulletin of Volcanology*, **67**, pp. 811–815.

CARTER, A. J., GIRINA, O., RAMSEY, M.S. DEMYANCHUK, Y. V., 2008, ASTER and field observations of the 24 December 2006 eruption of Bezymianny Volcano, Russia. *Remote Sensing of Environment*, **112**, pp. 2569–2577.

CHIEN, S., SILVERMAN, D., DAVIES, A. G., MCLAREN, D., MANDL, D. AND HEGEMIHLE, J. 2010, Onboard Instrument Processing Concepts for the HyspIRI Mission. *IEEE International Geoscience and Remote Sensing Symposium, 2010.* 25-30 July, Honolulu, USA. [Online]. Available at: http://trs-new.jpl.nasa.gov/ dspace/bitstream/2014/41511/1/JPLPUB10-03.pdf [accessed: November 2010].

DANES, Z. F., 1972, Dynamics of lava flows. *Journal of Geophysical Research*, **77**, pp. 1430–1432.

DAVIES, A. G., CHIEN, S., BAKER V., DOGGETT, T., DOHM, J., GREELEY, R., IP, F., CASTANO, R., CICHY, B., RABIDEAU, G., TRAN, R. AND SHERWOOD, R., 2006, Monitoring active volcanism with the Autonomous Sciencecraft Experiment (ASE) on EO–1, *Remote Sensing of Environment*, **101**, pp. 427–446.

DAVIES, A. G., CALKINS, J., SCHARENBROICH, L., VAUGHAN, R. G., WRIGHT, R., KYLE, P., CASTAŃO, R., CHIEN, S., TRAN, D., 2008, Multi–instrument remote and in situ observations of the Erebus Volcano (Antarctica) lava lake in 2005: A comparison with the Pele lava lake on the jovian moon Io. *Journal of Volcanological Geothermal Research*, **177**, pp. 705–724.

DONEGAN, S. AND FLYNN, L.P.,, 2004 Comparison of the response of the Landsat 7 Enhanced Thematic Mapper + and the Earth Observing–1 Advanced Land Imager over active lava flows. *Journal of Volcanological Geothermal Research,* **135**, pp. 105– 126.

DOZIER, J., 1981, A method for satellite identification of surface temperature fields of subpixel resolution. *Remote Sensing of Environment*, **11**, pp. 221– 229.

DRAGONI, M., BONAFEDE, M. AND BOSHI, E., 1986, Downslope flow models of a Bingham liquid: Implications for lava flows. *Journal of Volcanological Geothermal Research*, **30**, pp. 305–325.

EOSDIS, 2010. *An Overview of EOSDIS.* [Online]. Available at: http://esdis.eosdis.nasa.gov/eosdis/overview.html [accessed November, 2010].

FISHER, W. A., MOZHAM, R. M., POLCYN, F. AND LANDIS, G. H., 1964, Infrared surveys of Hawaiian Volcanoes, *Science*, **146**, pp. 733–742 (Abstract).

FLYNN, L., 1992, Radiative Temperature Measurements of the Pu'u 'O'o–Kupaianaha Eruption with Implications for Satellite Remote Sensing, PhD Dissertation, University of Hawaii at Manoa.

FLYNN, L., P., 1996, *Thermal Anomaly Low Spatial resolution*. EOS Volcanology Team Data Product Document MOU81–3292, 3rd draft (University of Hawaii, Manoa)

FLYNN, L., P. and MOUGINIS–MARK, P. J., 1992, Cooling rate of an active Hawaiian Lava Flow from night–time spectroradiometer measurements. *Geophysical Research Letters*, **19**, pp. 1783–1786.

FLYNN, L. P., MOUGINIS–MARK, P. J. AND HORTON, K. A., 1994, Distribution of thermal areas on an active lava flow field: Landsat observations of Kilauea, Hawaii, July 1991. *Bulletin of Volcanology,* **56**, pp. 284–296.

FLYNN, L. P., HARRIS, A. J. L. AND WRIGHT, R., 2001, Improved identification of volcanic features using Landsat 7 ETM+. *Remote Sensing of Environment,* **78**,pp. 180–193.

FRANCIS, P. W. AND MCALLISTER, R., 1986, Volcanology from space; using Landsat Thematic Mapper data in the Central Andes. EOS, *Transactions–American Geophysical Union,* **67**, pp. 170– 171.

FRANCIS, P. W. AND ROTHERY, D.A., 1987, Using the Landsat Thematic Mapper to detect and monitor active volcanoes: an example from Lascar volcano, Northern Chile. *Geology,* **15**, pp. 614– 617.

FRANCIS, P. AND ROTHERY, D., 2000, Remote Sensing of Active Volcanoes. *Annual Review of Earth Planet Science*, **28**, pp. 81–106.

GIGLIO, L. AND JUSTICE, C. O., 2003, Effect of wavelength selection on characterization of fire size and temperature. *International Journal of Remote Sensing*, **24**, pp. 3515–3520.

GIGLIO, L., CSISZAR, I., RESTÁS, A., MORISETTE, J., SCHROEDER, W., MORTON, D. AND JUSTICE, C., 2008, Active fire detection and characterization with the advanced spaceborne thermal emission and reflection radiometer (ASTER). *Remote Sensing of Environment*, **112**, pp. 3055–3063.

GLAZE, L., FRANCIS, P. W. AND ROTHERY, D. A., 1989, Measuring thermal budgets of active volcanoes by satellite sensing. *Nature*, **338**, pp. 144–146.

HARRIS, A. J. L., BUTTERWORTH, A. L., CARLTON, R. W., DOWNEY, I., MILLER, P., NAVARRO, P., AND ROTHERY, D. A., 1997, Low cost volcano surveillance from space: case studies from Etna, Krafla, Cerro Negro, Fogo, Lascar and Erebus. *Bulletin of Volcanology*, **59**, pp. 49–64.

HARRIS, A. J. L., FLYNN, L. P., KESZTHELYI, L., MOUGINIS–MARK, P. J., ROWLAND, S. K., AND RESING, J. A., 1998, Calculation of lava effusion rates from Landsat TM data. *Bulletin of Volcanology*, **60**, pp. 52−71.

HELLMAN, M. J. AND RAMSEY, M. S., 2004, Analysis of hot springs and associated deposits in Yellowstone National Park using ASTER and AVIRIS remote sensing. *Journal of Volcanological Geothermal Research,* **135**, pp. 195–219.

HIRN, B., DI BARTOLLA, C. AND FERRUCCI, F., 2005, Automated, Multi–Payload, High–Resolution Temperature Mapping and Instant Lava Effusion Rate Determination at Erupting Volcanoes. International Geoscience and Remote Sensing Symposium, 2005. Proceedings, 25–29 July, **7**, pp. 5056–5059.

IWASAKI, A. AND FUJISADA, H., 2005, ASTER Geometric Performance. *IEEE T Geoscience and Remote Sensing*, **43**, pp. 2700–2706.

JPL, 2010. *NASA 2009 HyspIRI Science Workshop Report*. JPL Publication 10-3. [Online]. Available at: http://hyspiri.jpl.nasa.gov/downloads/public/2009_Workshop/2009%20HyspIRI%20Science%20Workshop%20Report-final.pdf [accessed: November, 2010].

KATO, M., SYOJ, M. AND OYANAGI, M., 2001, *ASTER Status and Data Application Use*. 22nd Asian Conference on Remote Sensing, 5–9 November, 2001, Singapore.

LOMBARDO, V., BUONGIORNO, M. F., PIERI, D., MERUCCIA, L., 2004, Differences in Landsat TM derived lava flow thermal structures during summit and flank eruption at Mount Etna. *Journal of Volcanological Geothermal Research*, **134**, pp. 15– 34.

LOMBARDO, V. AND BUONGIORNO, M. F., 2006, Lava flow thermal analysis using three infrared bands of remote–sensing imagery: A study case from Mount Etna 2001 eruption. *Remote Sensing of Environment*, **101**, pp. 141–149.

LOMBARDO, V., HARRIS, A. J. L., CALVARI, S. AND BUONGIORNO, M. F., 2009, Spatial variations in lava flow field thermal structure and effusion rate derived from very high spatial resolution hyperspectral (MIVIS) data. *Journal of Geophysical Research*, **114**, B02208, doi:10.1029/2008JB005648.

MATSON, S., SHCNEIDER, S. R., ALDRIDGE, B. AND SATCHELL, B., 1984, *Fire Detection using the NOAA–series satellites*. Washington DC: National Oceanic and Atmospheric Adminisatation. NOAA Technical Report NESDIS 7.

MATTHEWS, S., GARDEWEG, M., SPARKS, R., 1997, The 1984 to 1996 cyclic activity of Lascar Volcano, northern Chile: cycles of dome growth, dome subsidence, degassing and explosive eruptions. *Bulletin of Volcanology*, **59**, pp. 72–82.

MORISETTE, J. T., GIGLIO, L., CSISZAR, I. AND JUSTICE, C. O., 2005, Validation of the MODIS active fire product over Southern Africa with ASTER data. *International Journal of Remote Sensing*, **26**, pp. 4239–4264.

MOUGINIS–MARK, P., ROWLAND, S., FRANCIS, P., FRIEDMAN, T., GARBEIL, H., GRADIE, J., SELF, S., WILSON, L., CRISP, J., GLAZE, L., JONES, K., KAHLE, A., PIERI, D., KRUEGER, A., WALTER, L., WOOD, C., ROSE, W., ADAMS, J., AND WOLFF, R., 1991, Analysis of active volcanoes from the Earth Observing System. *Remote Sensing of Environment*, **36**, pp. 1–12.

OPPENHEIMER, C., 1991, Lava flow cooling estimated from Landsat Thematic Mapper Infrared data: the Lonquimay eruption (Chile, 1989). *Journal of Geophysical Research,* **96**, pp. 21 865– 21 878.

OPPENHEIMER, C., 1993, Thermal distributions of hot volcanic surfaces constrained using three infrared bands of remote sensing data. *Geophysical Research Letters*, **20**, pp. 431–434.

OPPENHEIMER, C., FRANCIS, P. W., ROTHERY, D. A. AND CARLTON, R. W. T., 1993, Infrared Image Analysis of Volcanic Thermal Features: Láscar Volcano, Chile, 1984–1992. *Journal of Geophysical Research*, **98**, pp. 4269–4286.

PIERI, D. AND ABRAMS, M., 2004, ASTER watches the world's volcanoes: a new paradigm for volcanological observations from orbit. *Journal of Volcanological Geothermal Research,* **135**, pp. 13–28.

PIERI, D. AND ABRAMS, M., 2005, ASTER observations of thermal anomalies preceding the April 2003 eruption of Chikurachki volcano, Kurile Islands, Russia. *Remote Sensing of Environment*, **90**, pp. 84–97.

PIERI, D. C., CRISP, J AND KAHLE, A. B., 1995, Observing Volcanism and Other Transient Phenomena with ASTER. *Journal of the Remote Sensing Society of Japan*, **15**, pp. 56–61.

PLANCK, M., 1901, On the Law of Distribution of Energy in the Normal Spectrum. *Annalen der Physik*, **4**, pp. 553–563. In German.

QIN, Z., KARNIELI, A. AND BERLINER, P., 2002, Remote sensing analysis of the land surface temperature anomaly in the sand–dune region across the Israel–Egypt border. *International Journal of Remote Sensing*, 23, pp. 3991–4018.

RAMSEY, M., S. AND DEHN, J., 2004, Spaceborne observations of the 2000 Bezymianny, Kamchatka eruption: the integration of high–resolution ASTER data into near real–time monitoring using AVHRR. *Journal of Volcanological Geothermal Research*, **135**, pp. 127–146.

ROSE, S. AND RAMSEY, M., 2009, The 2005 eruption of Kliuchevskoi volcano: Chronology and processes derived from ASTER spaceborne and field-based data. *Journal of Volcanology and Geothermal Research*, **184**, pp. 367–380.

ROTHERY, D. A., 1988, The need for volcano monitoring and the ability to detect activity using emitted short wavelength infrared. International *Geoscience and Remote Sensing Symposium*: 'Remote Sensing: Moving Toward the 21st Century', 12–16 Sep 1988.

ROTHERY, D. A., FRANCIS, P. W., WOOD, C. A.,, 1988, Volcano monitoring using short wavelength infrared data from satellites. *Journal of Geophysical Research*, **93**, pp. 7993–8008.

SALISBURY, J. W., WALTER, L. S., & D'ARIA, D., 1988, *Midinfrared, (2.5 to 13 μm) spectra of igneous rocks*. USGS open file report (pp. 88–686).

SHAW, H. R. AND SWANSON, D. A., 1970, *Eruption and flow rates of flood basalts*, in Proceedings 2nd Columbia River Basalt Symposium, p271–299, E. Washington State College Press, Cheney, WA.

STEFAN, J., 1879, Über die Beziehung zwischen der Wärmestrahlung und der Temperatur. *Sitzungsberichte der mathematisch–naturwissenschaftlichen Classe der kaiserlichen Akademie der Wissenschaften*, **79**, pp. 391–428.

TASSI, F., AGUILERA, F., VASELLI, O., MEDINA, E., TEDESCO, D., DELGADO HUERTAS, A. POREDA, R AND KOJIMA, S., 2009, The magmatic– and hydrothermal–dominated fumarolic system at the Active Crater of Lascar volcano, northern Chile. *Bulletin of Volcanology*, **71**, pp. 171–183.

UNIVERSITY OF WYOMING, 2008, *Upper Air Data, Soundings*. [Online]. Available at: http://weather.uwyo.edu/upperair/sounding.html (accessed: Sept 2010).

VAN MANEN, S. M AND DEHN, J., 2009, Satellite remote sensing of thermal activity at Bezymianny and Kliuchevskoi from 1993 to 1998. *Geology*, **37**, pp. 983–986.

VAUGHAN, R. G. AND HOOK, S. J., 2006, Using satellite data to characterize the temporal behavior of an active volcano: Mount St. Helens, WA. *Geophysical Research Letters*, 33, L20303, doi: 10.1029/2006GL027957.

VAUGHAN, R. G., KESZTHELYI, L. P., DAVIES, A. G., SCHNEIDER, D. J., JAWOROWSKI, C., HEASLER, H., 2010, Exploring the Limits of Identifying Sub–pixel Thermal Features using ASTER TIR Data, *Journal of Volcanological and Geothermal Research*, **189**, pp. 225–237.

WESSELS, R., SENYUKOV, S., TRANBENKOVA, A., RAMSEY, M. AND SCHENIDER, D., 2004, *Detecting small geothermal features at Northern Pacific volcanoes with ASTER thermal infrared data.* (Abstract). American Geophysical Union Fall Meeting, December 13–17, 2004.

WIEN, W., 1896, Uber die Energieverteilung in Emissionspektrum eines schwarzen Korpers. *Annals of Physics,* **58**, pp. 662–669.

WOOSTER, M. J., 2001, Long–term infrared surveillance of Lascar Volcano: contrasting activity cycles and cooling pyroclastics. *Geophysical Research Letters*, **28**, pp. 847–850.

WOOSTER, M. J., 2002, Small–scale experimental testing of fire radiative energy for quantifying mass combusted in natural vegetation fires. *Geophysical Research Letters*, **2921**, doi:10.1029/2002GL015487.

WOOSTER, M. J., 2007, Remote sensing: sensors and systems. *Progress in Physical. Geography*, **31**, pp. 35–100.

WOOSTER, M. J. AND ROTHERY, D. A., 1997, Thermal monitoring of Lascar Volcano, Chile, using infrared data from the along–track scanning radiometer: a 1992–1995 time series. *Bulletin of Volcanology*, **58**, pp. 566–579.

WOOSTER, M. J. AND KANEKO, T., 2001, Testing the accuracy of solar reflected radiation corrections applied during satellite thermal analysis of active volcanoes. *Journal of Geophysical Research,* **106**, pp. 13 381–13 394.

WOOSTER, M. J., ROTHERY, D.A., SEAR, C.B. AND CARLTON, R.W., 1998, Monitoring the development of active lava domes using data from the ERS–1 Along Track Scanning Radiometer. *Advances in Space Research*, **21**, pp. 501–505.

WOOSTER, M. J., KANEKO, T., NAKADA, S. AND SHIMIZU, H., 2000, Discrimination of lava dome activity styles using satellite derived thermal structures. *Journal of Volcanological Geothermal Research*, **102**, pp. 97–118.

WRIGHT, R. AND FLYNN L. P., 2003, On the retrieval of lava–flow surface temperatures from infrared satellite data. *Geology*, **31**, pp. 893–896.

WRIGHT, R. AND FLYNN L. P., 2004, A space–based estimate of the volcanic heat flux into the atmosphere during 2001 and 2002. *Geology*, **32**, pp. 189–192.

WRIGHT, R., ROTHERY, D. A., BLAKE, S., HARRIS, A. J. L. AND PIERI, D. C., 1999, Simulating the response of the EOS Terra ASTER sensor to high temperature volcanic targets. *Geophysical Research Letters*, **26**, pp. 1773–1776.

WRIGHT, R., FLYNN, L., P., GARBEIL, H., HARRIS, A., J., L. AND PILGER, E., 2004, MODVOLC: near–real–time thermal monitoring of global volcanism. *Journal of Volcanological Geothermal Research*, **135**, pp. 29–49.

WRIGHT, R., CARN, S. A. AND FLYNN, L. P., 2005, A satellite chronology of the May–June 2003 eruption of Anatahan volcano. *Journal of Volcanological Geothermal Research*, **146**, pp. 102–116.

WRIGHT, R., GARBEIL, H. AND DAVIES, A.G., 2010, Cooling rate of some active lavas determined using an orbital imaging spectrometer. *Journal of Geophysical Research*, **115**, DOI:10.1029/2009JB006536.

YAMAGUCHI, Y., KAHLE, A. B., TSU, H., KAWAKAMI, T. AND PNIEL, M., 1998, Overview of Advanced Spaceborne Thermal Emission and Reflection Radiometer (ASTER). *IEEE Transactions on Geoscience and Remote Sensing*, **36**, pp. 1062–1071.

YAMAGUCHI, Y., FUJISADA, H., KAHLE, A. B., TSU, H., KATO, M, WATANABE, H., SATO, I AND KUDOH, M., 2001, ASTER Instrument Performance, Operation Status and Application to Earth Sciences. *International Geoscience and Remote Sensing Symposium, 2001*, 9–13 July 2001, **3**, pp. 1215–1216.

FIGURES
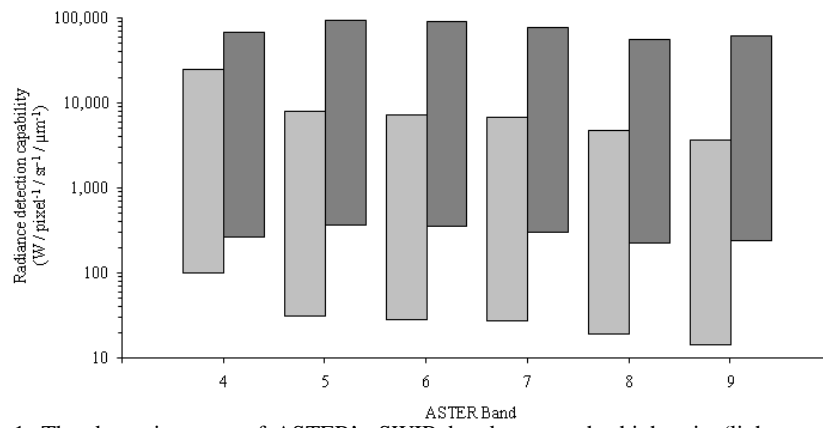
Fig. 1. The dynamic range of ASTER's SWIR bands set to the high-gain (light-grey) and second low-gain (dark-grey) modes; the extreme settings of the sensor. Radiance signals outside these ranges remain un-quantified, with saturation above and no useful measurement below. Note log-scale of y-axis. (Data from Abrams *et al.*, 2002).
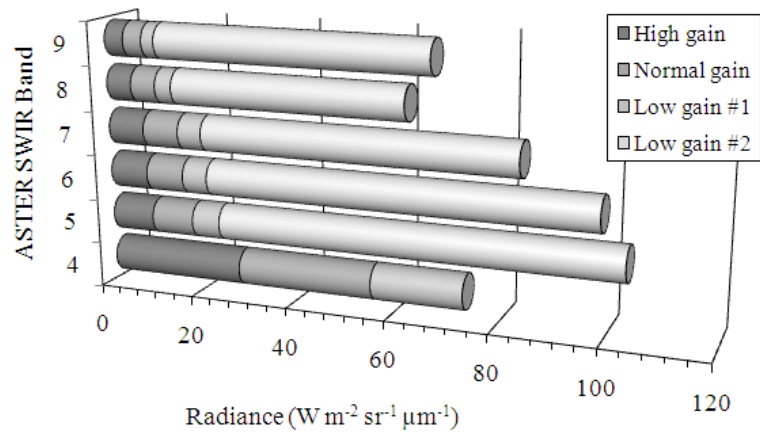
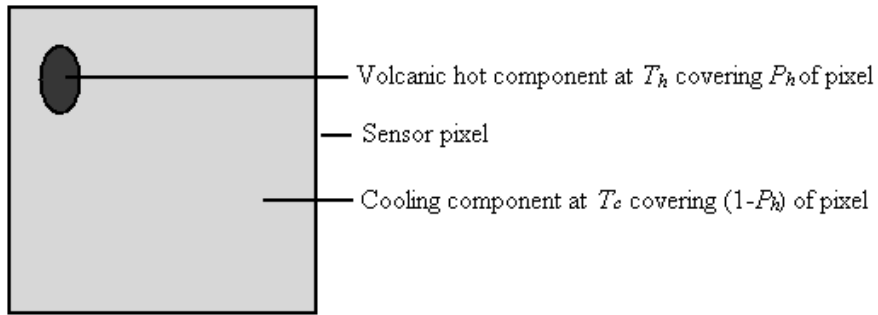Fig. 2. Maximum radiance measurable in ASTER's SWIR bands when set to the varying gain settings available (note that only three settings are available for band 4).

Fig. 3. A theoretical two-component pixel imaging a volcanic hotspot (at temperature T_h and with a sub-pixel proportional area of P_h) within a homogeneous cooler surface of temperature T_c and sub-pixel proportional area of $1-P_h$.
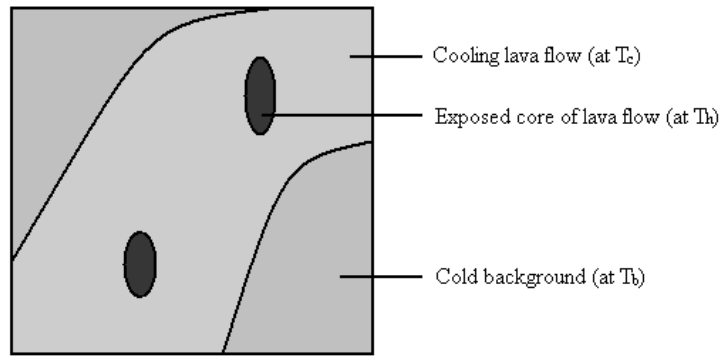
Fig. 4. A theoretical pixel imaging a lava-flow consisting of three-distinct thermal components of temperature: T_h, T_c and T_b, as envisaged by Oppenheimer (1993).
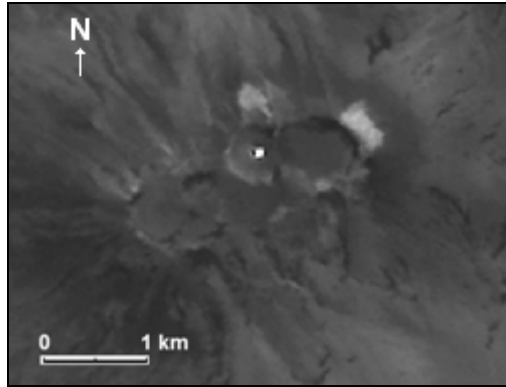
Fig. 5. Daytime ASTER SWIR image (September 16, 2003) of Lascar Volcano (Chile). Note the glow emanating from the active lava dome found within the volcano's central crater.
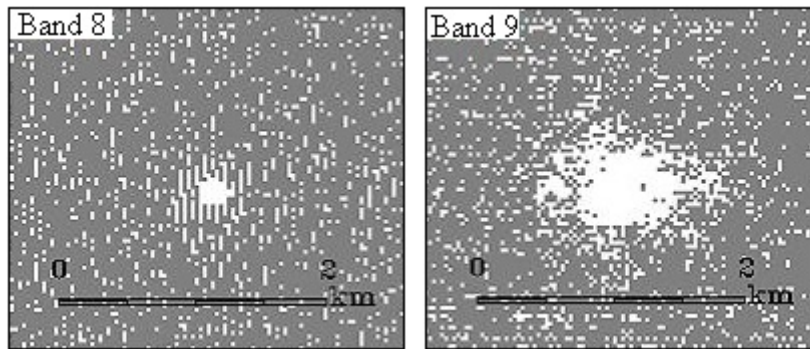
Fig. 6. Night-time SWIR ASTER imagery of the thermally anomalous surface at Lascar, Chile, on 11 June, 2003. The band 8 image was acquired using the second low-gain setting while the band 9 image was obtained using the high-gain setting. The greater spatial extent of the thermal anomaly in the high-gain band 9 image is evident.
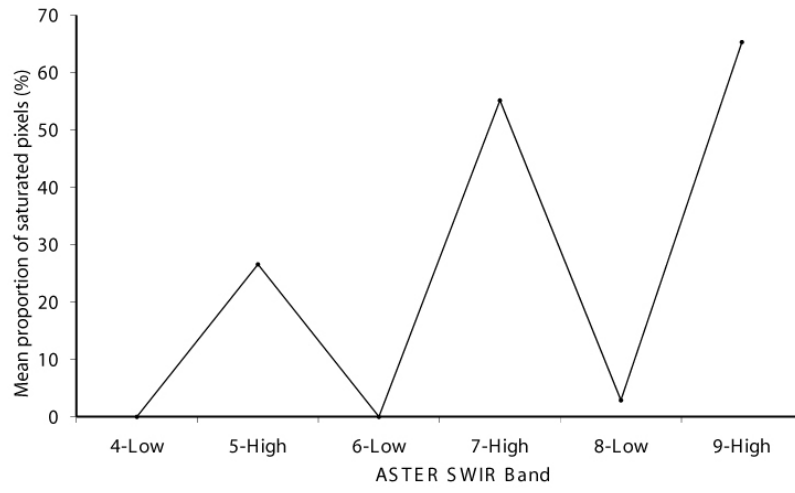
Fig. 7. The mean proportion of saturated pixels found within alternating gain ASTER SWIR imagery of Lascar, based on the dataset detailed in table 1.
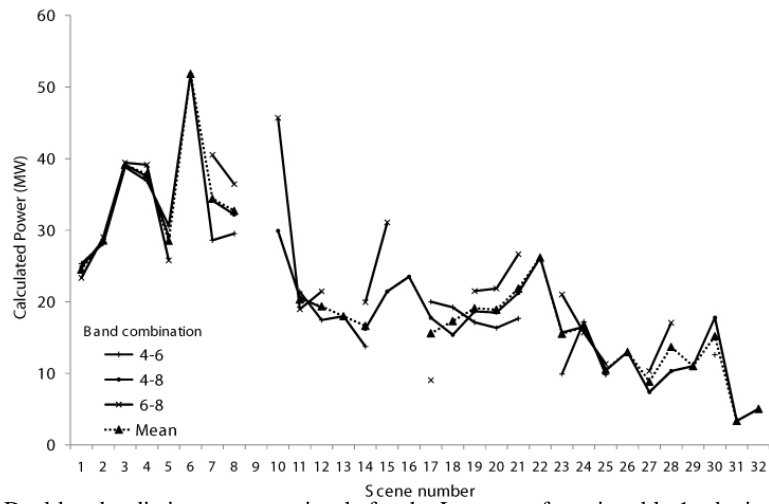
Fig. 8. Dual-band radiative power retrievals for the Lascar surfaces in table 1, obtained using differing combinations of all low-gain (even) ASTER SWIR bands. Gaps indicate that no solution was possible.
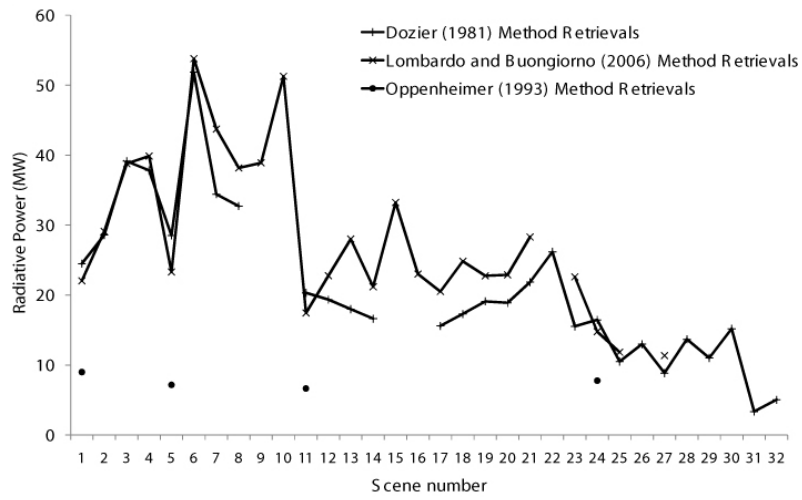
Fig. 9. Comparison between two–component (Dozier and Lombardo and Buongiorno methods) and three–component (Oppenheimer method) power retrievals for the Lascar surfaces in table 1, assuming $T_h = 1073$ K where required.. Gaps indicate no solution was possible.
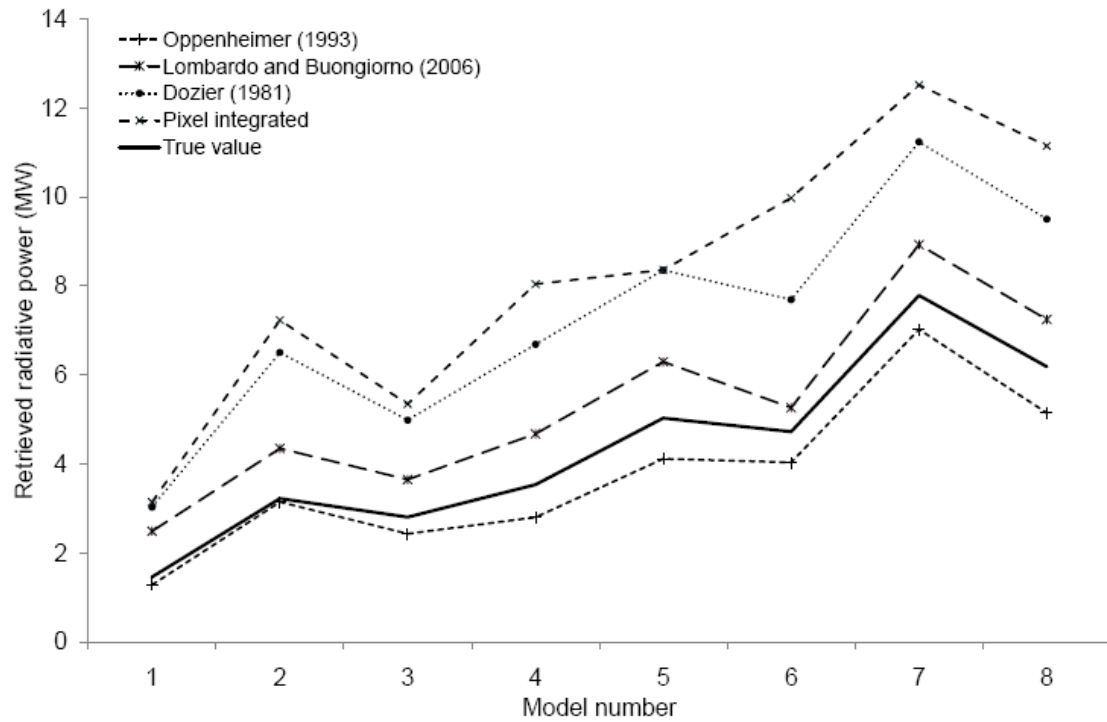
Fig. 10. Radiative power retrievals of the Dozier, Oppenheimer and Lombardo and Buongiorno Methods applied to simulated scenarios (Models 1-8, see Table 3) and based on the assumption of $T_h = 1073$ K and where relevant, $T_b = 300$ K. Also plotted is the true radiant power that such a surface, theoretically would emit along with that retrieved based on the use of pixel-integrated data from ASTER SWIR band 9 (2.395 µm).
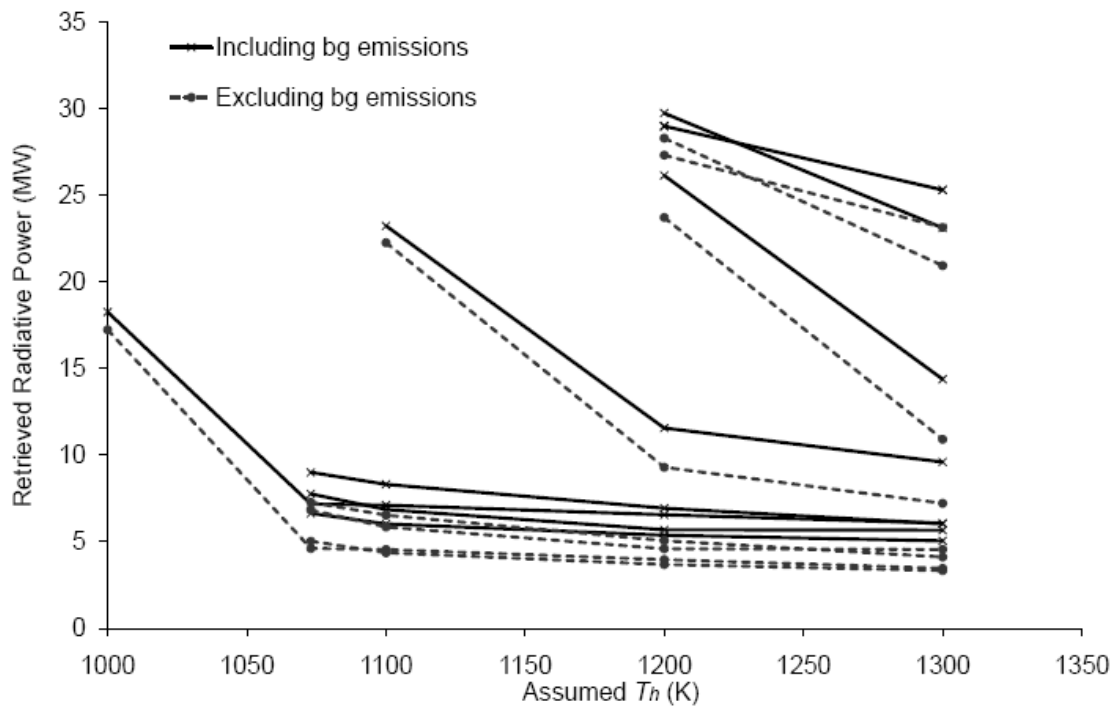
Fig. 11. The influence that the assumption of varying T_h has on Oppenheimer Method radiative power retrievals for the Lascar time series in Table 1. Only those with more than one temperature producing a retrieval are plotted and here, retrievals both including and excluding emissions from the background surface are shown. Emissions from the background are calculated simply by applying the Stefan-Boltzmann Law to the characteristics of the derived background component.
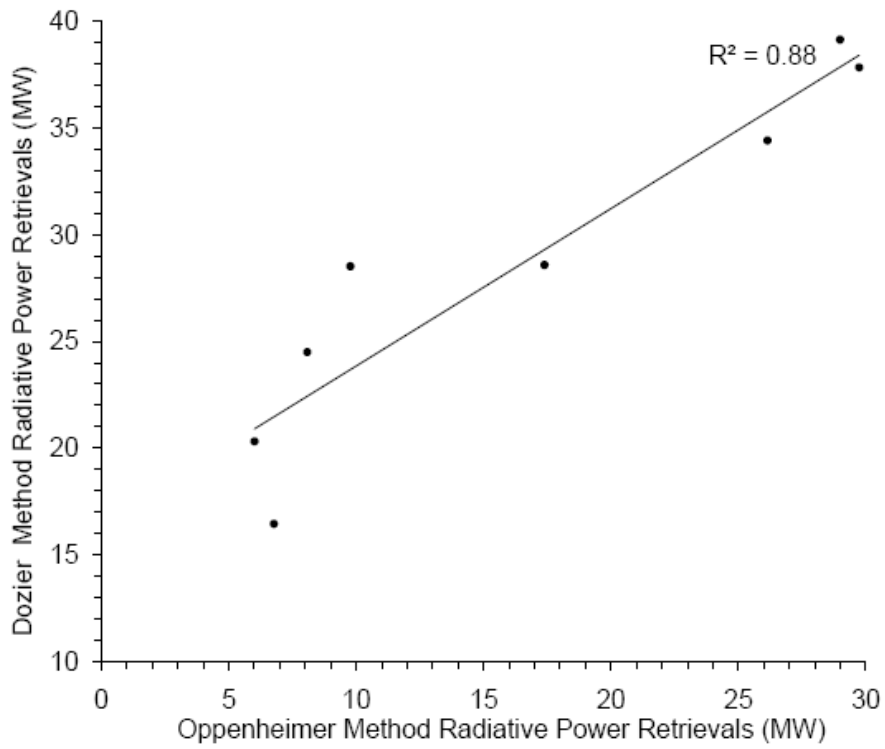
Fig. 12. The mean of the Oppenheimer Method radiative power retrievals Table 3, plotted against the corresponding mean radiative power retrievals of the Dozier Method. The data consist of Oppenheimer Method retrievals that include from the background region. Emissions from the background are calculated simply by applying the Stefan-Boltzmann Law to the characteristics of the derived background component.
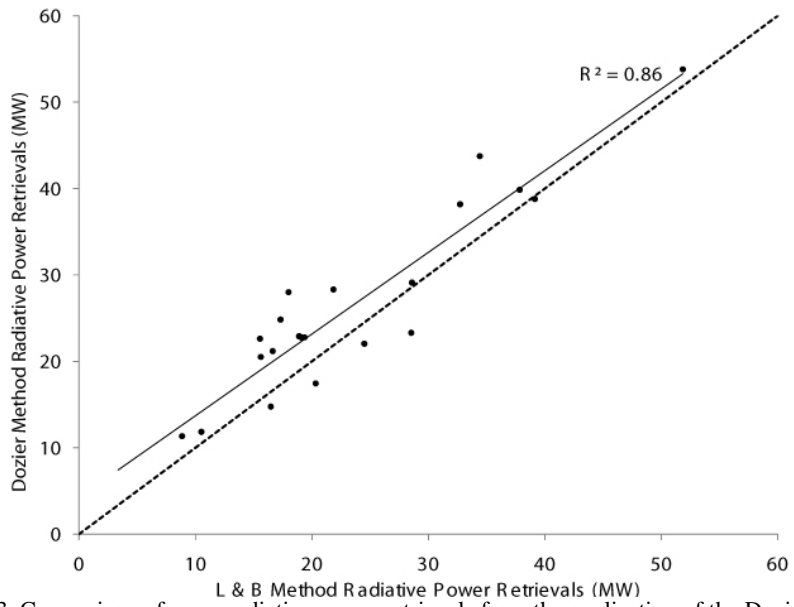
Fig. 13. Comparison of mean radiative power retrievals from the application of the Dozier and Lombardo and Buongiorno (L & B) Methods for Lascar data. The intermittent line represents the 1:1 relationship.
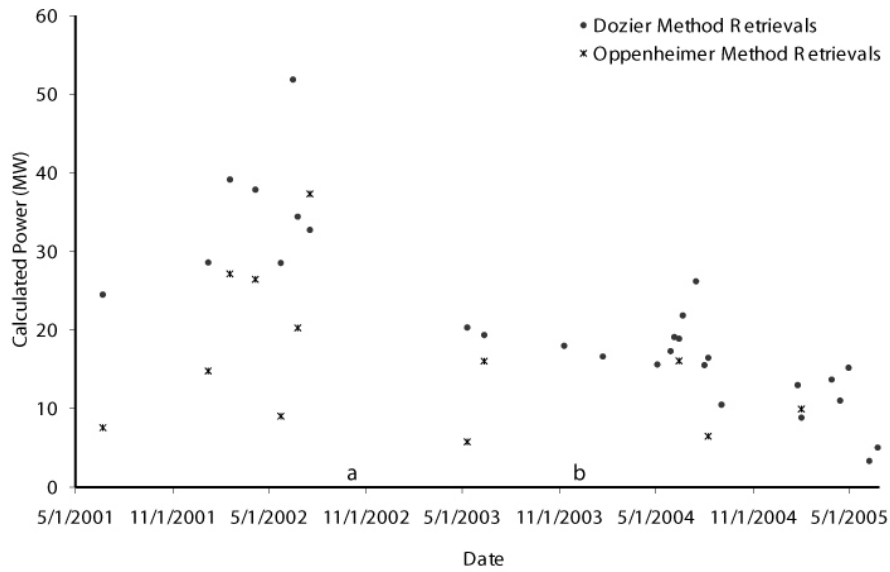
Fig. 14. Temporal trends in mean ASTER radiative power retrievals, following application of the Dozier and Oppenheimer Methods for the five-year Lascar time-series. The labelled points a and b are discussed in text. Plotted data consist of 12 retrievals for the Oppenheimer method and 31 for the Dozier method.

TABLES

Table 1. Dates of night-time ASTER SWIR scenes imaging Lascar volcano, Chile, in the absence of cloud obscuration. Scenes obtained from Dr. Matt Watson of the University of Bristol and the Earth Observing System Data and Information System (EOSDIS, 2010). Prior to the removal of cloudy scenes, this dataset consisted of data from 2000-2005.

Scene number	L1B ASTER Images	Scene number	L1B ASTER Images
1	2001-06-21	17	2004-05-03
2	2002-01-06	18	2004-05-28
3	2002-02-16	19	2004-06-04
4	2002-04-05	20	2004-06-13
5	2002-05-23	21	2004-06-20
6	2002-06-15	22	2004-07-15
7	2002-06-24	23	2004-07-31
8	2002-07-17	24	2004-08-07
9	2002-10-05	25	2004-09-01
10	2003-01-02	26	2005-01-23
11	2003-05-10	27	2005-01-30
12	2003-06-11	28	2005-03-28
13	2003-11-09	29	2005-04-13
14	2004-01-21	30	2005-04-29
15	2004-01-28	31	2005-06-07
16	2004-03-09	32	2005-06-23

Table 2. Atmospheric transmissivity values determined for each ASTER SWIR band, on a seasonal basis. Data are derived from radiosonde data taken from Antofagasta, Chile (273 km west of Lascar). Source: University of Wyoming (2008).

ASTER Band:	4	5	6	7	8	9
Peak Wavelength(s) (µm):	1.658	2.170	2.217	2.272	2.313 & 2.340	2.403
Lascar Summer	0.99	0.99	0.99	0.99	0.99	0.99
Lascar Spring	0.99	0.99	0.99	0.99	0.97	0.96
Lascar Autumn	0.99	0.99	0.99	0.99	0.99	0.99
Lascar Winter	0.99	0.99	0.99	0.99	0.99	0.99

Table 1. Characteristics of surfaces modelled with four to seven thermal components (P_x and T_x represent the proportion and temperature of that component of the pixel, respectively).

Model Number	Component 1		Component 2		Component 3		Component 4		Component 5		Component 6		Component 7	
	P_x	T_x	P_x	T_x	P_x	T_x	P_x	T_x	P_x	T_x	P_x	T_x	P_x	T_x
1	0.0001	1073	0.1	600	0.15	500	0.7499	300	-	-	-	-	-	-
2	0.0001	1073	0.15	700	0.05	800	0.799	300	-	-	-	-	-	-
3	0.0001	1073	0.1	700	0.15	600	0.3	400	0.4499	300	-	-	-	-
4	0.00001	1073	0.05	900	0.2	600	0.25	400	0.49999	300	-	-	-	-
5	0.0001	1073	0.05	800	0.15	750	0.25	500	0.25	400	0.2999	300	-	-
6	0.00001	1073	0.05	950	0.15	700	0.2	500	0.25	400	0.34999	300	-	-
7	0.0001	1073	0.0999	900	0.05	800	0.1	750	0.2	600	0.25	400	0.3	300
8	0.00001	1073	0.05	950	0.1	800	0.15	600	0.2	500	0.5	400	0.29999	300

Table 4. Oppenheimer Method radiative power retrievals in terms of the range of solutions obtained following the assumption of a range of T_h values. Scene numbers correspond with those in Table 1. Emissions from the background are calculated simply by applying the Stefan-Boltzmann Law to the characteristics of the derived background component.

Scene number	Radiative power range excluding background (MW)	Radiative power range including background (MW)	Assumed T_h range from highest to lowest (K)
1	5.06 - 7.27	6.94 - 9.00	1200 - 1073
2	9.30 - 22.26	11.56 - 23.23	1200 - 1100
3	27.31	28.99	1200
4	28.29	29.74	1200
5	3.96 - 17.23	6.56 – 18.26	1200 - 1000
6		------- Saturated -------	
7	23.72	26.14	1200
8		-	
9		-	
10		------- Saturated -------	
11	3.68 - 5.03	5.37 - 6.64	1200 - 1073
12		-	
13		------- Saturated -------	
14		-	
15		------- Saturated -------	
16		------- Saturated -------	
17		-	
18		-	
19		-	
20		-	
21		-	
22		-	
23		-	
24	4.59 - 6.82	5.69 - 7.76	1200 - 1073
25		-	
26		-	
27		-	
28		-	
29		-	
30		-	
31		-	
32		-	